Profile Studies of Ion-Implanted MESFET's

J. M. MICHAEL GOLIO AND ROBERT J. TREW, MEMBER, IEEE

Abstract—A study of ion-implanted MESFET performance as a function of the implantation energy and fluency, and including the effects of deep-level trapping-state concentrations in the substrate, has been conducted. Carrier concentrations as a function of depth are determined through the use of LSS theory and a profiling model. An analytic device model, which computes both dc and RF characteristics, is then employed to predict MESFET performances. The study includes the effects of depth-dependent transport properties and has indicated a number of design rules for the fabrication of optimized ion-implanted devices.

I. Introduction

THE PERFORMANCE of FET's fabricated by ion implantation depends greatly on carrier concentrations and velocity-field characteristics as a function of depth into the active device layers. The presence of deep-level traps in the semiconductor contributes to the complexity of problems associated with the characterization of ion-implanted devices.

This paper presents the results of a study to determine the effects of various concentration and transport profiles upon device performance. The study utilizes theoretical models of both material properties and device characteristics. This information is combined with an experimental material characterization to provide improved quantitative accuracy of the model.

Fig. 1 outlines the modeling steps involved in obtaining the results to be presented. Initially, the determination of typical ranges for concentrations of deep-level trapping states $N_T(x)$ was made from a novel measurement technique using both differential capacitance and conductance DLTS data. Shallow-level donor concentrations $N_D(x)$ were then determined from LSS theory as a function of implantation parameters. These concentrations as a function of depth were then used in a profiling model to determine the free-carrier profile $n(x)$ for the material. Carrier transport properties were also determined from the trap and donor profiles. This was done through the use of Monte Carlo particle simulations and a model to account for the effects of compensation in the semiconductor.

An analytic model which utilizes all of this information is then used to assess performance potential. The dc characteristics and small-signal S-parameters along with figures-of-merit are computed by the model. The distinction between free-carrier and donor profiles, the effect of deep-level traps, and the depth dependence of mobility and velocity are shown to be important considerations which have been ignored in previous models.

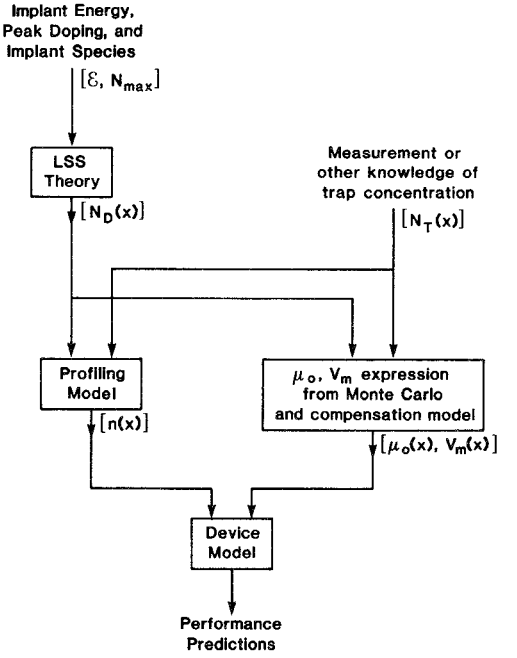

Fig. 1. Flowchart of modeling steps required to obtain study results.

II. The Device Model

A one-dimensional analytic device model with a small-signal analysis has been developed and utilized for this work. The model is based upon the principles presented by Pucel [1] but has been generalized for arbitrary doping profiles and includes differences in the free-carrier and shallow-level donor profiles and the effects of deep-levels.

The model assumes that the electron transport properties of a material can be simulated by a two-piece velocity-field relationship. The two-piece approximation is defined from a theoretical velocity-field characteristic determined by Monte Carlo techniques. For electric fields less than an appropriate saturation field E_m, the electron velocity is described by a linear expression

$$v = \mu_0 E. \tag{1}$$

For electric fields above E_m, the electrons move at a constant maximum velocity v_m.

The low-field mobility as a function of depth into the channel is determined from [2]

$$\mu_0 = \frac{\mu_{\max}}{1 + \left[\dfrac{\log N_D^1}{N_0}\right]^C} (1-\Theta)^b \tag{2}$$

Manuscript received May 2, 1983; revised August 3, 1983. This work was supported by Rockwell International Electronics Research Center and the U.S. Army Research Office under Contract DAAG29-80-K-0080.

The authors are with the Electrical and Computer Engineering Department, North Carolina State University, Raleigh, NC 27650.

0018-9480/83/1200-1066$01.00 ©1983 IEEE

where

$$N_D^1 = N_D \cdot m^3$$
$$\mu_{max} = 8380 \text{ cm/V} \cdot \text{s}$$
$$N_0 = 23.2553$$
$$C = 23.0$$
$$\Theta = N_T/N_D$$

and

$$b = \begin{cases} A(\log N_D)^2 - B(\log N_D) + C, & \text{for } N_D > 10^{21} \text{ m}^{-3} \\ 0.114992, & \text{for } N_D < 10^{21} \text{ m}^{-3} \end{cases}$$

with

$$A = 0.025$$
$$B = 0.817278$$
$$C = 6.252838$$

and where N_D is given in m^{-3}.

Equation (2) gives the low-field mobility as a function of donor density and background compensation. To derive (2), the theoretical results of Walukiewicz *et al.* [3] were used in conjunction with Monte Carlo velocity-field predictions [4]. The Monte Carlo results were used to determine the mobility as a function of background donor density with no traps present, and the Walukiewicz values were then normalized to the Monte Carlo numbers. The normalized data were finally curve fit to obtain (2). Very good agreement is obtained when (2) is plotted against the normalized Walukiewicz values as shown in Fig. 2.

The technique for determining the maximum velocity v_m has been previously presented [5]–[7]. The saturation velocity can be described by the expression

$$v_m = v_0 - A \log\left[(1-y)^2 + B \cdot y\right] \tag{3}$$

where

$$y = \left[N_D(x)/N_0\right]^{2.5}$$
$$N_0 = 1.5 \times 10^{22} \text{ m}^{-3}$$
$$A = 0.0262$$
$$B = 0.4$$

and

$$v_0 = 1.40 \times 10^5 \text{ m/s}.$$

Equation (3) gives v_m in 10^5 m/s when $N_D(x)$ is expressed in m^{-3}. The expression is assumed to have the same dependence upon compensation ratio Θ as (2). Thus the factor $(1-\Theta)^b$ is multiplied with (3) to obtain v_m in the presence of traps. The exponent b is defined in (2).

Equations (2) and (3), in conjunction with knowledge of the three profiles ($n(x)$ is the free-electron concentration, $N_D(x)$ is the donor concentration, and $N_T(x)$ is the deep-level concentration), allow for the derivation of a device model which includes the effects of varying transport properties as a function of epi-depth. The profiles of interest are determined with a novel characterization technique [2] that combines experimental capacitance–voltage (CV) and conductance deep-level transient spectroscopy (DLTS) data. The experimental equipment and procedure is discussed elsewhere [8].

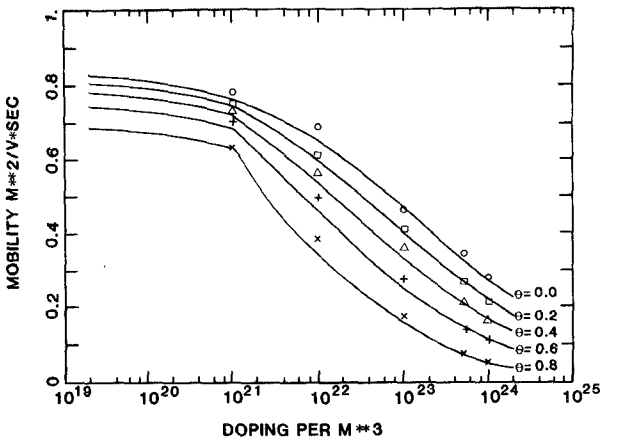

Fig. 2. Low-field mobility as a function of doping and deep-level compensation. The solid lines are computed from (2) for $\Theta = 0.0$, 0.2, 0.4, 0.6, 0.8. The data points are from the normalized theoretical computations [3].

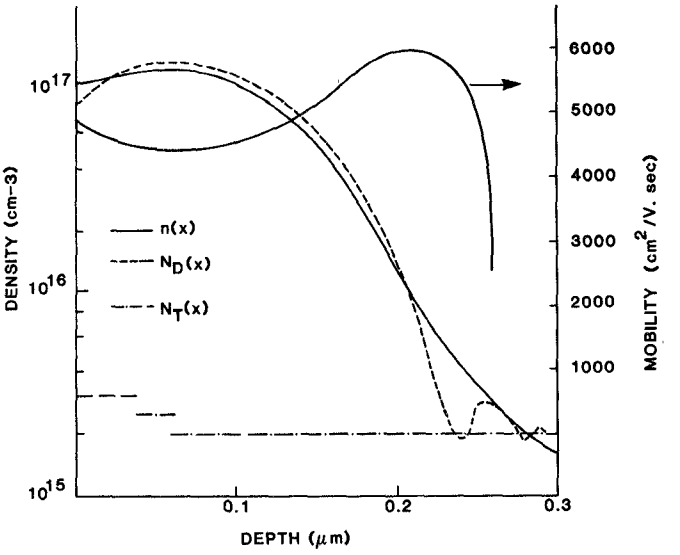

Fig. 3. Resulting concentration profiles and low-field mobility profile for one device.

For this work, an ion-implanted 1-μm gate-length device [9] was analyzed. The experimental characterization revealed the presence of a dominant deep-level donor state 0.736 eV below the conduction band. The level is probably EL2 [10], [11] in agreement with the findings of Martin *et al.* [12]. The resulting free-carrier, shallow-level donor, and deep-level concentrations as a function of depth into the material are shown in Fig. 3. Despite the scatter of the data near the tail, it is evident that diffusion of the electrons has caused the free-carrier and shallow-level donor concentrations to differ significantly. The low-field mobility versus depth obtained from this analysis is also shown in Fig. 3. In regions of relatively high donor concentration, the mobility varies inversely with doping, as expected. Near the tail of the implanted region, however, the deep-levels seriously degrade the mobility acting to confine the active device channel.

The dc $I-V$ characteristics for the device, as determined from the model, are compared in Fig. 4 with the measured

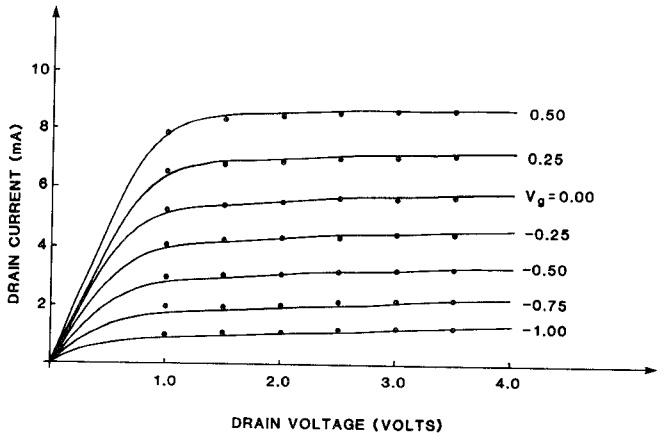

Fig. 4. Comparison of model predicted and measured $I-V$ characteristics for a 1-μm ion-implanted device.

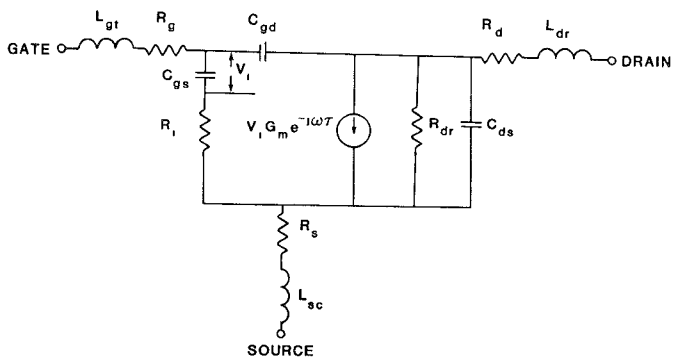

Fig. 5. The equivalent circuit for an FET used in the analysis.

$I-V$ curves. It should be noted that without the inclusion of the effects of traps upon the carrier transport characteristics, the excellent agreement shown in Fig. 4 could not be obtained. The traps have a tendency to "soften" the pinchoff characteristics of the device (i.e., when traps are included in the simulation, the slope dI_D/dV_g is not as great near the pinchoff). For all of the devices studied in this work, this "softening" effect was required to obtain best agreement with the measured $I-V$ characteristics.

The model allows the element values for a small-signal equivalent circuit as shown in Fig. 5 to be determined. The equivalent circuit can be analyzed to obtain RF performance predictions as a function of the various implantation parameters and material characteristics.

III. Results

The results that follow were obtained following the modeling steps outlined in Section I and illustrated in Fig. 1. Three parameters were varied independently. They are 1) implantation energy ϵ, 2) peak doping density $N_{\max}$, and 3) trapping state density $N_T(x)$. The implant species was assumed to be Si in GaAs and the activation was assumed to be 100 percent for all devices. The gate length of the simulated devices is 1 μm with a gate width of 300 μm. The trapping state density was assumed to be constant as a function of depth for these studies. Note that the peak doping density can be converted to a corresponding ion

TABLE I
Ion-Implanted MESFET Equivalent Circuit Element Values
$\epsilon = 75$ KEV, $N_{\text{peak}} = 2\times10^{17}$ cm^{-3}, $V_{ds} = 3.0$ V, and $I_d = I_{dss}$

	Deep-Level Concentration		
Element	1×10^{14} cm^{-3}	2×10^{15} cm^{-3}	1×10^{16} cm^{-3}
g_m(mmho)	46.4	45.6	41.5
C_{gs}(pF)	0.419	0.417	0.399
Rdr(kΩ)	1.22	1.20	1.35
R_I(Ω)	3.337	3.423	3.680
τ(psec)	8.00	8.16	8.41
f_{max}(GHz)	66.1	64.5	61.8

The remaining parameters were constant with the values C_{ds} = 0.0577 pF, C_{gd} = 0.0432 pF, R_I = 1.214 Ω and R_s = 1.214 Ω.

fluency through the simple relationship

$$\Theta = \sqrt{2\Pi}\,\sigma_p N_{\max} \tag{4}$$

where σ_p is the standard deviation of the projected range. The value for σ_p can be obtained from LSS theory when the implant schedule is known.

Fig. 6(a) shows the computed carrier profiles for the same 75-keV implant with $N_{\max} = 2\times10^{17}$ cm^{-3}, but for three different trapping state concentrations. The low-field mobility and maximum velocity profiles corresponding to these three cases are shown in Fig. 6(b). It is clear from the figures that the trapping state concentration in the material has a significant effect on both the free-carrier concentration and the transport properties of the implanted material. The equivalent circuit element values that correspond to these cases are shown in Table I. The deep-level concentration has the most effect upon the device transconductance, which decreases as the trap concentration increases, and the gate delay time, which increases with the trap concentration.

For the implant energy and peak doping studies, the trapping state density was left constant at $N_T = 2\times10^{15}$ cm^{-3}. This number was chosen to be in general agreement with the results shown in Fig. 3. The implant energy was varied from 50–150 keV while the peak doping took values between 8×10^{16} and 4×10^{17} cm^{-3}.

The value for f_T is computed from first-order considerations to be given by

$$f_T = \frac{g_m}{2\Pi C_{gs}}. \tag{5}$$

The quantity $f_{\max}$ is obtained by noting the frequency at which Mason's unilateral gain (as predicted by the model) goes to unity. Mason's unilateral gain at a frequency of 10 GHz is plotted as a function of energy in Fig. 8. The results clearly indicate the superiority of low-energy implants for high-frequency operation.

The information plotted in Fig. 8 indicates the importance of implant energy to achieve optimum high-frequency performance. Notice that for a peak doping of 4×10^{17} cm^{-3}, a decrease of implant energy from 150 to 50 keV results in better than a 9-percent increase in the unilateral

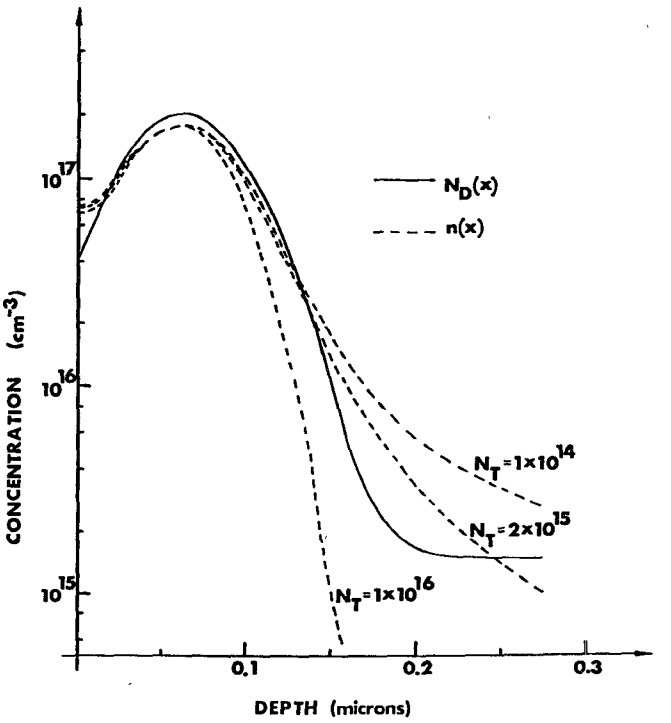

Fig. 6. (a) Concentration profiles for a 75-keV implant with $N_{max}=2\times10^{17}$ cm^{-3} and with $N_T=1\times10^{14}$, 2×10^{15}, and 1×10^{16} cm^{-3}. The solid curve is the donor density, while the dashed curves are free-carrier densities appropriate for the various trapping state densities. (b) Transport property profiles for the three 75-keV implants of Fig. 6(a). The solid curves give low-field mobility as a function of depth. The dashed curves give maximum velocity as a function of depth.

power gain, from 16.2 to 17.7 dB. The superior high-frequency performance of low-energy implants is easily understood in terms of the device physics. The available

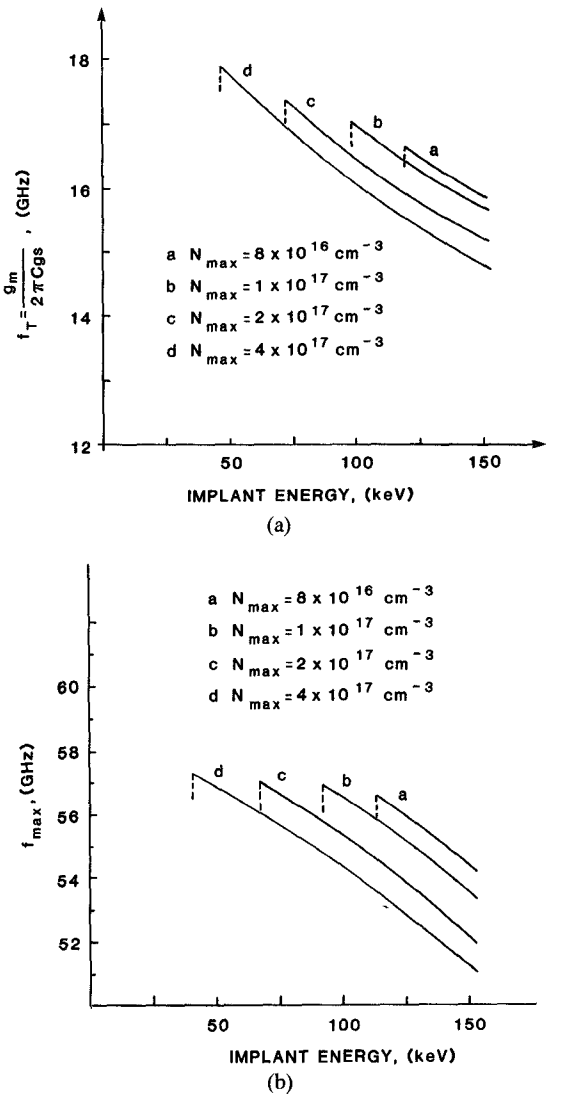

Fig. 7. (a). Predicted gain–bandwidth product f_T versus implantation energy ϵ. The peak doping N_{max} is used as an independent parameter. (b). Predicted maximum frequency of oscillation f_{max} versus implantation energy ϵ. The peak doping N_{max} is used as an independent parameter.

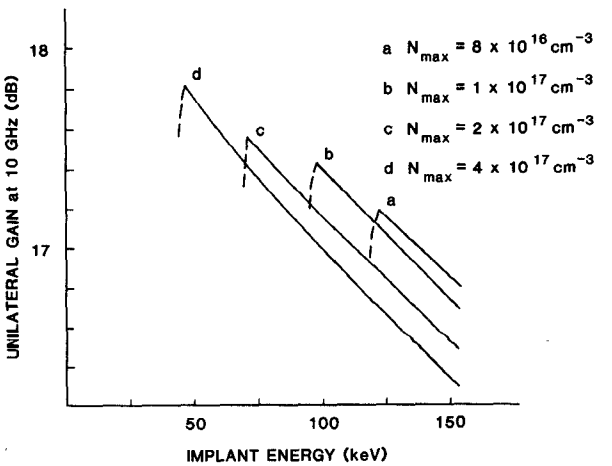

Fig. 8. Mason's unilateral gain U at 10 GHz versus energy ϵ. Trapping state density is constant at $N_T=2\times10^{15}$ cm^{-3}.

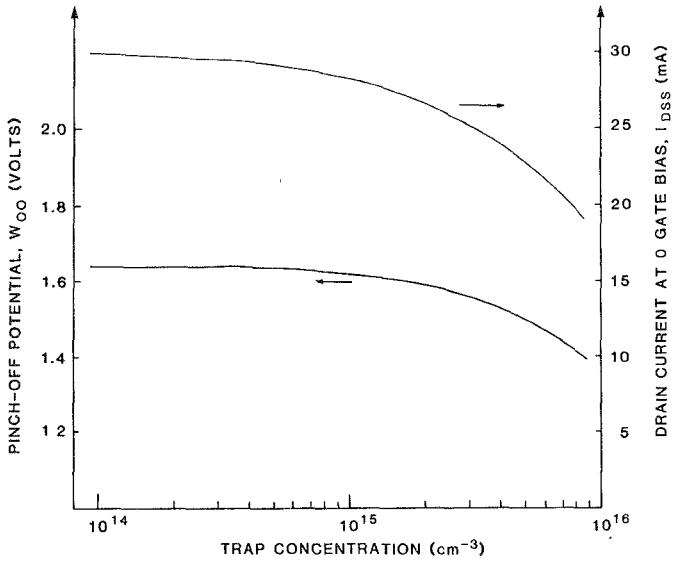

Fig. 9. Predicted effects of varying trapping state concentrations on dc characteristics.

charge carriers lie closer to the surface (gate contact) for low-energy implants. Thus the gate potential required to alter the depletion width is smaller than for deep implants and the transconductance of the device should rise. High transconductance is important to the high-frequency performance of these devices. All of the devices considered in compiling Figs. 7 and 8 were compared at a bias of $I_D = 10$ mA. The dashed line falling off rapidly at the low-energy end of the curves indicate that for energies lower than this $I_{DSS} < 10$ mA.

The trapping state concentration in ion-implanted semiconductor material can vary over a wide range of values. The quality of the initial semi-insulating substrate, the temperature characteristic of the various processing steps used, and the type of annealing implemented all affect the kinds and relative concentrations of deep-levels in the final device [13], [14]. For the trap study in this work, an implant energy of 75 keV and a peak doping density of 2×10^{17} cm^{-3} was assumed. The background trapping state concentration was varied from 0 to 10^{16} cm^{-3}. For trapping state concentrations above 10^{16} cm^{-3}, the device would be normally pinched off.

Fig. 9 illustrates the effects traps have on the zero gate bias current I_{DSS}, and the pinch off potential W_{00}. The trapping state density of the figure ranges between 10^{14} and 10^{16} cm^{-3}. Over this range, the zero gate bias current varies between 30 and 18 mA, while the pinchoff potential varies between 1.62 and 1.38 V. This large range of dc characteristics indicates that reproducibility will be a problem unless consistency of the trapping state density in the substrate can be maintained. It should be further noticed that for deep-level concentrations below a level of about 10^{15} cm^{-3}, very little change in the characteristics occurs. As the trapping state concentration increases above the low 10^{15} cm^{-3} level, however, the current and pinchoff potential begin to fall rapidly.

Fig. 10 shows the pinchoff "softening" effect mentioned

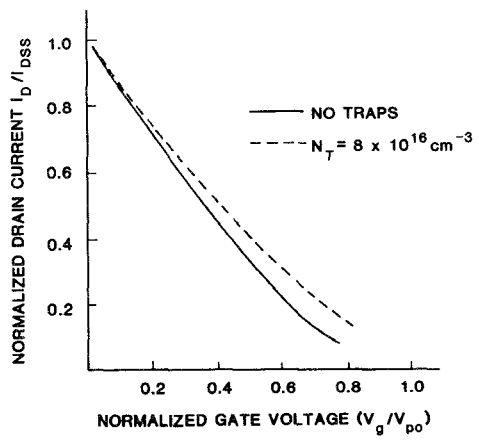

Fig. 10. Normalized drain current predictions versus normalized gate voltage with and without traps.

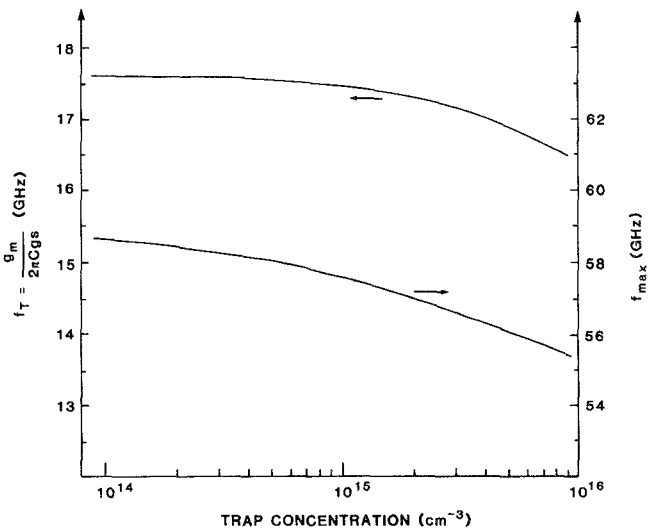

Fig. 11. Predicted gain–bandwidth product f_T and maximum frequency of oscillation f_{max} versus background trapping state concentration.

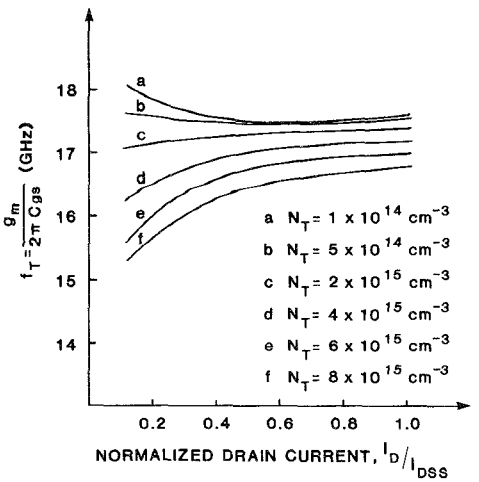

Fig. 12. Predicted gain–bandwidth product f_T as a function of normalized drain current. The background trapping state concentration is used as a variable parameter.

in the previous section for one particular device. Notice that the figure plots normalized current and voltage. Thus the trapping density affects the dc characteristics of the device in a qualitative, as well as a quantitative, way.

Deep-level traps also have some effect on the RF performance of the device, as illustrated in Figs. 11 and 12. Fig. 11 shows clearly the decrease of f_T and f_{max} associated with increasing trapping state concentrations—especially for deep-level concentrations above the low 10^{15} cm^{-3} range. In Fig. 12, note that for low-bias currents, f_T increases when few traps are present while it decreases for higher trap concentrations. This is easily explained in terms of the degrading effects traps have on mobility and velocity. As the gate bias restricts current flow, a larger fraction of the carriers are forced deeper into the channel. This corresponds to the more lightly doped regions of the device. If the compensation ratio is fairly small (i.e., few traps) then from (1) and (3) the transport properties are superior, and f_T increases. If, on the other hand, the trapping state density is on the same order of magnitude as the shallow-level donor concentration, then the compensation ratio approaches one. This corresponds to extreme degradation of mobility and velocity and thus forces f_T to decrease.

IV. Conclusions

It has been shown how deep-level traps in ion-implanted devices degrade carrier transport properties in the semiconductor material. The degradation is more severe near the tail of the implant profile than near the peak. Thus the transport properties of the device will be depth, or bias, dependent. A modeling technique which accounts for this dependence has been used to study device properties as a function of fabrication parameters and deep-level concentrations. The results indicate that low-energy implants should possess superior high-frequency properties, and that lowering the trapping state density in the material should improve device performance. For the 75-keV implant studied in this work, a critical deep-level concentration of about 10^{15} cm^{-3} was identified. For trapping state concentrations above this level, performance degradation becomes increasingly severe. Decreasing deep levels in ion-implanted devices below this critical trapping state concentration should improve device performance. It should be noted, however, that for a different implant schedule than the one considered here (i.e., 75 keV with $N_{max} = 2 \times 10^{17}$ cm^{-3}) the critical trap density may be different.

References

[1] R. A. Pucel, H. Statz, and H. A. Haus, "Signal and noise properties of gallium arsenide microwave field-effect transistors," *Advances in Electronics and Electron Physics*. New York: Academic, vol. 38, 1975, pp. 195–265.

[2] J. M. Golio, R. J. Trew, H. Lefevre, and G. N. Maracas, "A characterization technique for ion-implanted GaAs MESFET's," submitted for publication.

[3] W. Walukiewicz, L. Lagoaski, L. Jastrzebski, M. Lichtensteiger, and H.C. Gatos, "Electron mobility and free-carrier absorption in GaAs: Determination of the compensation ratio," *J. Appl. Phys.*, vol. 50, pp. 899–908, Feb. 1979.

[4] M. A. Littlejohn, J. R. Hauser, and T. H. Glisson, "Velocity-field characteristics of GaAs with $\Gamma_6 - L_6 - X_6$ conduction-band ordering," *J. Appl. Phys.*, vol. 48, pp. 4587–4590, Nov. 1977.

[5] J. M. Golio, "Compound semiconductors for microwave MESFET applications," *M. S. thesis*, North Carolina State University, Raleigh, NC, May 1980.

[6] J. M. Golio and R. J. Trew, "Compound semiconductors for low-noise microwave MESFET applications," *IEEE Trans. Electron Devices*, vol. ED-27, pp. 1256–1262, July 1980.

[7] J. M. Golio and R. J. Trew, "Profile studies of ion-implanted MESFET's," in *1983 IEEE Microwave Millimeter Wave Monolithic Circuits Symp. Dig.*, May 31–June 1, 1983, pp. 22–26.

[8] J. M. Golio, G. N. Maracas, R. J. Trew, and N. A. Masnari, "A technique for modeling ion-implanted GaAs MESFET's in the presence of deep levels," presented at the 1983 Cornell Conference on High Speed Semiconductor Devices and Circuits, Aug. 1983.

[9] B. M. Welch, Y. D. Shen, R. Zucca, R. C. Eden, and S. I. Long, "LSI processing technology for planar GaAs integrated circuits," *IEEE Trans. Electron Devices*, vol. ED-27, pp. 1116–1124, June 1980.

[10] C. Kocot and C. A. Stolte, "Backgating in GaAs MESFET's," *IEEE Trans. Microwave Theory Tech.*, vol. MTT-30, pp. 963–968, July 1982.

[11] G. M. Martin, J. P. Farges, G. Jacob, and J. P. Hallais, "Compensation mechanisms in GaAs," *J. Appl. Phys.*, vol. 51, pp. 2840–2852, May 1980.

[12] G. M. Martin, A. Mitonneau, and A. Mircea, "Electron traps in bulk and expitaxial GaAs crystals," *Electron. Lett.*, vol. 13, pp. 191–192, Mar. 31, 1977.

[13] S. G. Liu, E. C. Douglas, C. P. Wu, C. W. Magee, S. Y. Narayan, S. T. Jolly, F. Kolondra, and S. Jain, "Ion-implantation of sulfur and silicon in GaAs," *RCA Rev.*, vol. 41, pp. 227–262, June 1980.

[14] H. M. Hobgood, G. W. Eldridge, D. L. Barrett, and R. N. Thomas, "High-purity semi-insulating GaAs material for monolithic microwave integrated circuits," *IEEE Trans. Electron Devices*, vol. ED-28, pp. 140–149, Feb. 1981.

J. Michael Golio was born in Christopher, IL, on March 30, 1954. He received the B.S.E.E. degree from the University of Illinois, Urbana, in 1976, and the M.S.E. and Ph.D. degrees from North Carolina State University, Raleigh, in 1980 and 1983, respectively.

From 1976 to 1978, he was employed by the Watkins-Johnson Company, Palo Alto, CA, where he worked on the design and development of broad-band solid-state microwave oscillators and amplifiers. Since 1978, he has been at North Carolina State University, where he has been involved in semiconductor device modeling, including both two-dimensional numerical device simulation and the development of one-dimensional analytic models. Currently, he is doing post-graduate work at NCSU in the areas of nonequilibrium and radiation effects in compound semiconductor devices.

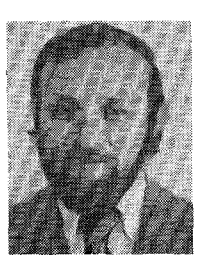

Robert J. Trew (S'71–M'74) was born in Saginaw, MI, on December 8, 1944. He received the B.E.E. degree from General Motors Institute, Flint, MI, in 1968, and the M.S.E. and Ph.D. degrees from the University of Michigan, Ann Arbor, in 1969 and 1975, respectively.

From 1971 to 1974, he was with the Electron Physics Laboratory of the University of Michigan, where he was involved in research on IMPATT and TRAPATT oscillators and amplifiers. From 1975 to 1977, he was engaged in the design and development of various types of solid-state microwave components while employed by the Watkins-Johnson Company, Palo Alto, CA. In 1977, he joined the faculty of North Carolina State University, Raleigh, NC, where he is currently an Associate Professor. His research interests are in the areas of microwave/millimeter-wave semiconductor devices and circuits.

Dr. Trew is a member of Sigma Xi, Eta Kappa Nu and Tau Beta Pi.